Field-induced incommensurate-to-commensurate transition in $Ba_2CuGe_2O_7$

A. Zheludev, S. Maslov, and G. Shirane

Brookhaven National Laboratory, Upton, New York 11973-5000

Y. Sasago, N. Koide, and K. Uchinokura

Department of Applied Physics, The University of Tokyo, 7-3-1 Hongo, Bunkyo-ku, Tokyo 113, Japan

(Received 19 May 1997)

We report an observation of a commensurate-incommensurate phase transition in the Dzyaloshinskii-Moriya spiral antiferromagnet $Ba_2CuGe_2O_7$. The transition is induced by an external magnetic field applied along the c axis of the tetragonal structure, i.e., in the plane of spin rotation. Bulk magnetic measurements and neutron-diffraction experiments show that the transition occurs in a critical field $H_c \approx 2.1$ T. Experimental results for the period of the magnetic structure and magnetization as functions of magnetic field are in quantitative agreement with our exact analytical solution for Dzyaloshinskii's model of commensurate-incommensurate transitions in spiral magnets. [S0163-1829(98)03206-8]

I. INTRODUCTION

Among relatively unusual and exotic magnetic interactions in solids is the Dzyaloshinskii-Moriya (DM) asymmetric exchange interaction.[1–3] Unlike the conventional Heisenberg exchange coupling, it is proportional to the *vector* product of interacting spins, and is permitted by symmetry only in noncentric crystal structures. It results from relativistic spin-orbit corrections[3] to the ordinary superexchange mechanism[4] and therefore is usually weak compared to antiferromagnetic symmetric exchange. This is why only few materials in which DM interactions play an important role have been found so far. The best known examples are cubic FeGe (Refs. 5,6) and MnSi,[7–9] where DM terms in the Hamiltonian cause an instability of ferromagnetic order towards the formation of an incommensurate spiral structure.

This paper deals with the properties of $Ba_2CuGe_2O_7$, a newly investigated system in which DM coupling plays a key role. Originally the magnetic properties of this quasi-two-dimensional (2D) antiferromagnet (AF) were investigated as part of the ongoing search for singlet ground-state compounds, triggered by the discovery of a spin-Peierls transition and other extraordinary magnetic properties of $CuGeO_3$.[10,11] While some materials related to $CuGeO_3$, e.g., $CaCuGe_2O_6$ (Refs. 12,13) and $BaCuSi_2O_6$,[14] have dimerized ground states and energy gaps in their spin-excitation spectra, $Ba_2CuGe_2O_7$ undergoes a transition to a magnetically ordered phase below $T_N \approx 3.2$ K and the magnetic excitations are gapless spin waves.[15] Even though the magnetic properties of $Ba_2CuGe_2O_7$ can be adequately described in terms of classical spins, they are rather intriguing: the magnetic structure is an incommensurate spin spiral. By performing detailed measurements of the spin-wave dispersion we have previously demonstrated that this spiral ordering may not be caused by competing exchange interactions.[15] Since $Ba_2CuGe_2O_7$ has a noncentric crystal structure, we have suggested that the incommensurate magnetic phase is a result of Dzyaloshinskii-Moriya interactions.

The crystal structure of $Ba_2CuGe_2O_7$, as well as the spiral spin arrangement in the magnetically ordered phase, were

discussed in detail in our previous work,[15] and only the essential features are reviewed here. The magnetic ($S=1/2$) Cu^{2+} ions are arranged on a square lattice in the (a,b) plane of the tetragonal structure [space group $P\bar{4}2_1m$ (No. 113), lattice constants $a=8.466$ Å, $c=5.445$ Å]. The in-plane interactions between spins are established through GeO_4 tetrahedra that, together with the Cu^{2+} ions, form distinct Cu-Ge-O layers. These layers are well isolated by interstitial nonmagnetic planes of Ba^{2+} ions. Only nearest-neighbor in-plane antiferromagnetic exchange interactions are important ($J \approx 0.48$ meV). Interplane coupling is ferromagnetic and substantially weaker ($J_\perp \approx 0.013$ meV). In the ordered phase the spins lie in the $(1,\bar{1},0)$ plane and the propagation vector for the spiral is $(1+\zeta,\zeta,0)$ where $\zeta=0.027$ [Fig. 1(a)]. The magnetic structure is a distortion of a Néel spin arrangement: a translation along the $(1,1,0)$ direction (hereafter referred to as the x axis) induces a rotation of the spins by an angle $\alpha = 2\pi/\zeta \approx 9.7°$ in the $(1,\bar{1},0)$ plane (relative to an exact antiparallel alignment). Along the $(1,\bar{1},0)$ direction (y axis) the spins are perfectly antiparallel. Nearest-neighbor spins from adjacent Cu planes are aligned parallel to each other.

The mechanism by which DM interactions can stabilize the spiral structure in $Ba_2CuGe_2O_7$ is illustrated in Fig. 1(b). The DM energy for two interacting spins S_1 and S_2 may be written as $(S_1 \times S_2) \cdot D^{(1,2)}$, where $D^{(1,2)}$ is the so-called Dzyaloshinskii vector attributed to the oriented bond between the two spins and $\times$ denotes a vector product. For spins lying in the $(1,\bar{1},0)$ plane the only relevant component of the vector D is D_y. The symmetry of the structure is such that for two subsequent Cu pairs (1,2) and (2,3) along the $(1,1,0)$ direction $D_y^{(1,2)}=D_y^{(2,3)}$ [Fig. 1(b)]. A finite value for D energetically favors a 90° angle between subsequent spins. Since AF exchange favors an angle of 180°, the total energy is minimized at some intermediate angle that is defined by the ratio of exchange and DM interactions strengths.

How can the mechanism described above be verified experimentally? If one could force the spins into the $(0,0,1)$ plane for example, D_y would become inactive, due to the
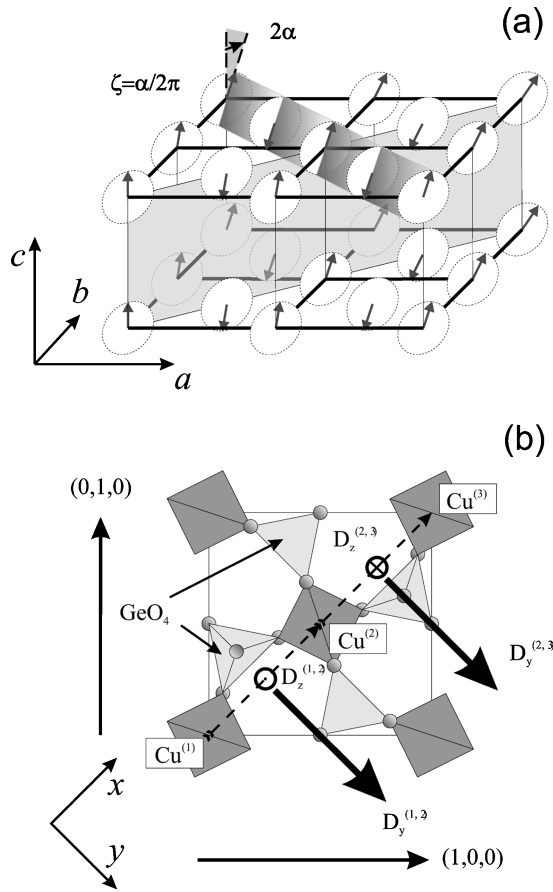
FIG. 1. (a) Magnetic structure of $Ba_2CuGe_2O_7$ (Ref. 15). (b) DM interactions in the Cu planes of $Ba_2CuGe_2O_7$. The $(1,-1,0)$ component of the Dzyaloshinskii vector **D** (solid arrows) is the same for all oriented Cu-Cu bonds (dashed arrow) along the $(1,1,0)$ direction. The z component is sign alternating.

nature of the vector product, and the incommensurate spiral would disappear. The z component of **D**, i.e., the $(0,0,1)$ projection, on the other hand, would become relevant. As shown in Fig. 1(b), for D_z, unlike for D_y, symmetry dictates a *change of sign* from one Cu-Cu bond to the next: $D_z^{(1,2)} = -D_z^{(2,3)}$. As a result, DM interactions would tend to distort the Néel spin arrangement towards a weak-ferromagnet (canted) structure, that is *commensurate* with the crystal lattice. In practice forcing spins into the (a,b) plane can be achieved by applying an external magnetic field along the c axis of the crystal. Indeed, in a structure with zero net magnetic moment spins tend to align perpendicular to the external field, which in the simplest case leads to spin-flop transitions in conventional antiferromagnets. In other words, if the proposed model for DM interactions in $Ba_2CuGe_2O_7$ is correct, we expect a field-induced commensurate-incommensurate magnetic transition (CI) in this material.

In the present paper we report an experimental observation of such a phase transition in $Ba_2CuGe_2O_7$ by means of bulk magnetization and neutron-diffraction measurements. We find that the phase transition is of rather unusual character and is the first "clean" realization of Dzyaloshinskii's model for CI transitions in spiral magnets induced by a magnetic field applied *in the plane of spin rotation*.[16] We also present an exact continuous-limit solution to Dzyaloshin-

skii's model. For the particular case of $Ba_2CuGe_2O_7$ theoretical predictions are in quantitative agreement with experimental data. A short preliminary report on this work is published elsewhere.[17]

II. EXPERIMENTAL PROCEDURES

Transparent, slightly yellowish single-crystal samples were prepared using the floating-zone method. Magnetization measurements were performed with a conventional dc superconducting quantum interference device magnetometer in the temperature range 2–300 K. Two sets of neutron-scattering experiments were carried out on the H4M (thermal beam) and H9 (cold beam) three-axis spectrometers at the High Flux Beam Reactor at Brookhaven National Laboratory on an irregularly shaped $\approx 4 \times 4 \times 4$ mm^3 single-crystal sample with a mosaic spread of $\approx 25'$. In the first set of measurements on H4M (experiment I) the H-T phase diagram was determined using neutrons of incident energy $E_i = 14.7$ meV with a $(20'-40'-20'-40')$ collimation setup and two PG filters. The second set of measurements was done on H9 (experiment II) and the field dependence of the magnetic propagation vector was studied using $(60'-40'-60'-\text{sample}-15'-80')$ collimations, an $E_i = 4.6$ meV neutron beam, and a Be filter in front of the sample. In both experiments the use of a pumped ^{4}He cryomagnet allowed us to work in the temperature range 1.3–5 K and magnetic fields up to 6.5 T. The sample was always mounted with the $(h,k,0)$ zone in the scattering (horizontal) plane and the field was applied along the vertical direction (c axis of the crystal).

The sample we used in preliminary experiments shattered when it was cooled down in the cryomagnet for the second time. We therefore tried to mount the new crystal as strain free as possible. The new sample was wrapped in aluminum foil that was attached to a thin Al plate. This technique has one serious drawback. As will be explained below, a good alignment of the crystallographic c axis with the magnetic field is crucial. Unfortunately, the described mounting procedure does not allow us to maintain an alignment of better than $\approx 1°$. Before the sample is put into the cryostat, an almost perfect alignment is achieved. It is upon cooling to base temperature that the undesirable misalignment occurs. In experiment I the $(1,-1,0)$ and $(1,1,0)$ crystallographic directions formed angles of 1.5° and 1° with the horizontal plane, respectively, as measured *in situ* at low temperature. In experiment II these angles were 1° and less than 0.3°, respectively.

III. EXPERIMENTAL RESULTS

A. Magnetization

The first evidence of a field-induced magnetic phase transition in $Ba_2CuGe_2O_7$ was found in bulk magnetic measurements. The longitudinal magnetization data collected at $T = 2$ K is plotted against magnetic field **H** applied along the a or c crystallographic axes in the inset in Fig. 2. For $\mathbf{H}\|\mathbf{a}$ no anomalies are observed. In contrast, when the field is applied along c, $M(H)$ has a broad steplike feature around $H = 2$ T. The anomaly is best seen in the plot $\chi(H)$ that was obtained
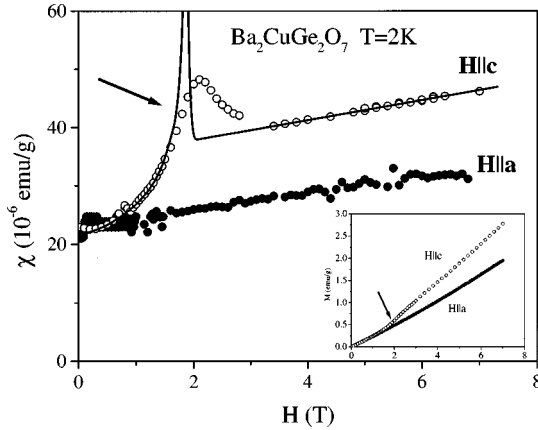
FIG. 2. Inset: Magnetization of single crystal $Ba_2CuGe_2O_7$ measured as a function of magnetic field applied along the c and a crystallographic axes. Main panel: Field dependence of magnetic susceptibility $\chi = dM/dH$ deduced from magnetization curves shown in the inset. The solid line represents a fit to the data, as described in the text.

by numerically differentiating the experimental magnetization curve (Fig. 2, main panel).

B. Neutron diffraction

The phase transition is best observed in neutron-diffraction experiments. Figure 3 (experiment II) shows some elastic scans along the $(1+\zeta,\zeta,0)$ direction measured in $Ba_2CuGe_2O_7$ at $T=1.4$ K. The different scans correspond to different values of magnetic field applied along the c axis. In zero field [Fig. 3(a)] the magnetic peak is positioned at $\zeta = 0.027$.[15] The incommensurability parameter ζ decreases gradually with increasing H. Around $H=1.8$ T an additional peak appears at the Néel point (1,0,0). At the same time the intensity of the satellite at $(1+\zeta,\zeta,0)$ starts to decrease rapidly and the rate at which ζ changes with field is increased [Fig. 3(b)]. On further increasing the field the central peak gains intensity and the satellite eventually vanishes at some critical field $H_c \approx 2.3$ T [Fig. 3(c)]. At higher fields only the Néel (commensurate) peak is seen, all the way up to the highest field available experimentally. The intensities of the $(1+\zeta,\zeta,0)$ satellite and the (1,0,0) peak are plotted against temperature in Fig. 3(d). Measured $\zeta(T)$ is shown in solid circles in Fig. 4.

C. Domains and sample alignment

The field-dependent behavior is *extremely* sensitive to the alignment of the crystallographic c axis with the applied field. The limitations of the sample-mounting technique employed, together with technical impossibility of adjusting the alignment *in situ* at low temperature, are therefore a serious experimental complication. This problem is closely linked to the issue of magnetic domains. In the tetragonal symmetry two spiral structures with propagation vectors $(1+\zeta,\zeta,0)$ and $(1+\zeta,-\zeta,0)$ are allowed. Zero-field cooling produces domains of equal volume. If the sample is cooled in an $H=1$ T field, that is removed only at low temperature, only one domain is present. Since we are able to exactly measure (but not adjust) the orientation of the sample *in situ*, we
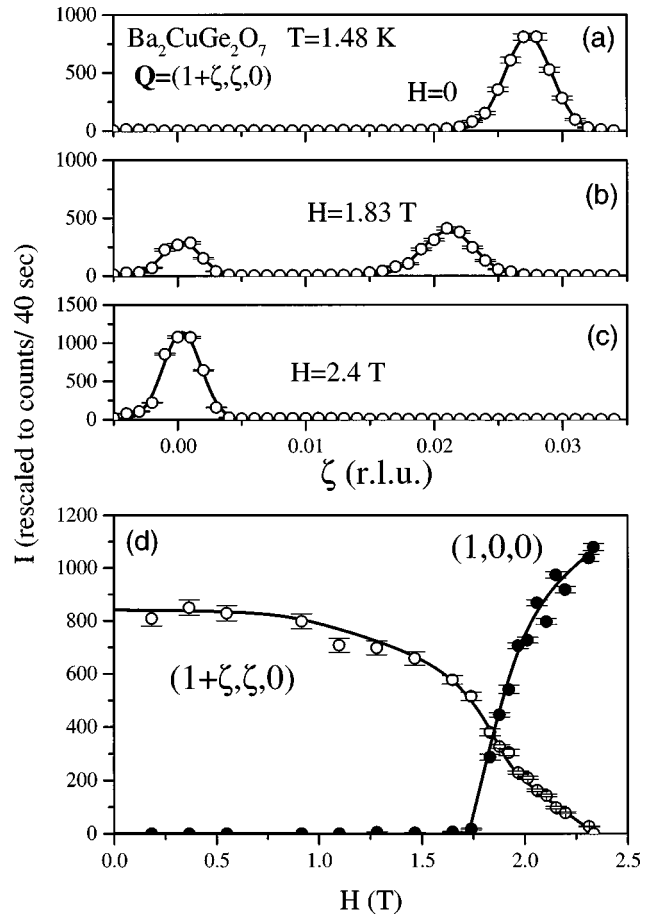

FIG. 3. (a)–(c) Elastic scans measured along the $(1+\zeta,\zeta,0)$ direction at $T=1.4$ K for several values of magnetic field applied along the c axis of the crystal. (d) Field dependence of the intensity in the (1,0,0) Néel peak (solid symbols) and the $(1+\zeta,\zeta,0)$ satellite (open circles).

could determine that it is the domain for which the plane of the spiral forms a larger angle with the applied field that is stabilized. This behavior can easily be explained. If the plane in which the spins are confined is not parallel to the external field, the system can gain some Zeeman energy without sacrificing much DM or exchange energy: all spins may tilt slightly in the direction of the field component normal to the spin plane, producing a cone structure with practically no change in the angles between neighboring spins. The domain for which the spin plane forms a larger angle with the applied field is thus energetically more favorable. Note that in the commensurate (high-field) structure there are also two possible domain types, with spins in the $(1,\bar{1},0)$ or (1,1,0) planes.

The data shown in Fig. 3 were collected on a field-cooled sample and the satellites correspond to the more misaligned $(1+\zeta,\zeta,0)$ domain (domain A, $\approx 1°$ tilt). No satellites were observed in the $(1+\zeta,-\zeta,0)$ domain (domain B, $<0.3°$ tilt) in any fields in field-cooling experiments. When the measurements at $T=1.4$ K were done on a zero-field-cooled sample, we observed that scattering intensities originating from both domains remain comparable in fields up to ≈ 1.7 T. At higher fields the Néel peak appears and domain B is rapidly destroyed. Applying a sufficiently large field thus brings us back to the situation where the entire crystal is a single magnetic domain.
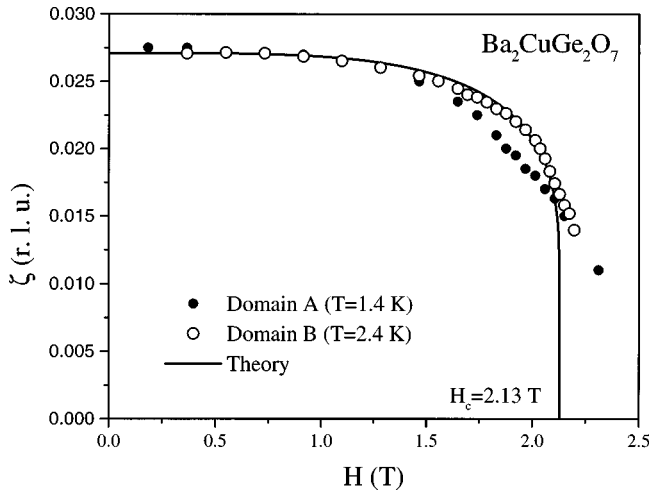
FIG. 4. Measured field dependence of the magnetic propagation vector ζ in the incommensurate phase of $Ba_2CuGe_2O_7$. The data shown by solid circles correspond to a domain misaligned by $\approx 1°$ with respect to the applied field, and were collected on a field-cooled sample at $T = 1.4$ K. Open circles are data points measured at $T = 2.4$ K in an almost perfectly aligned domain, obtained by zero-field-cooling the sample from $T = 5$ K. The solid line is a fit with a theoretical curve described in the Theory section.

D. Phase diagram

The experimental H-T phase diagram for $Ba_2CuGe_2O_7$ is shown in Fig. 5. The I-O-II line corresponds to the appearance of the magnetic reflection at the commensurate $(1,0,0)$ position. The III-O-IV line shows where the satellite peaks disappear. Both the O-II and the O-IV lines were measured in a field-cooled sample and the misalignment of the corresponding domain was $\approx 1.5°$ (experiment I).
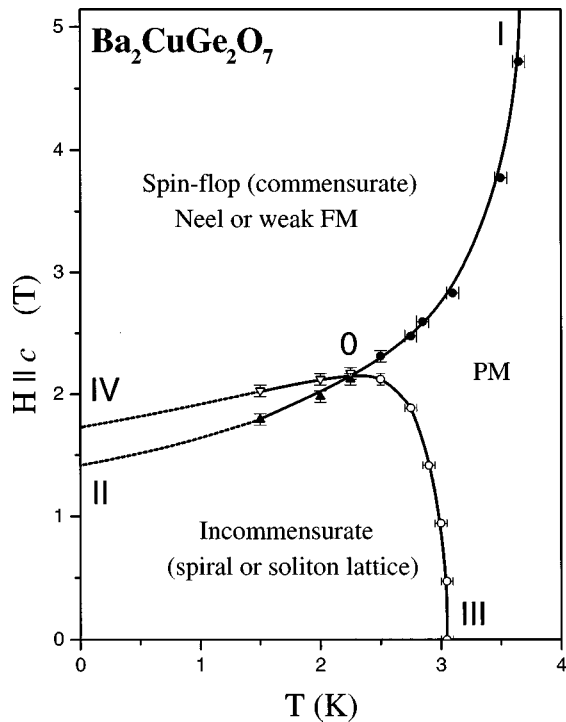

FIG. 5. Measured magnetic phase diagram of $Ba_2CuGe_2O_7$. The field is applied along the c axis of the crystal.

In the high-field phase the structure is commensurate, with a propagation vector $(1,0,0)$. This may be the signature of Néel order or (see introduction) a canted "weak ferromagnetic" structure. In the low-field region the structure is incommensurate with a propagation vector $(1+\zeta,\zeta,0)$. Only one domain is present since, as mentioned, field cooling was used. Note that except for the incommensurability of the low-field phase, the phase diagram strongly resembles that of an easy-axis Heisenberg antiferromagnet in external field applied along the easy axis.

In the II-O-IV region the Néel peak coexists with the incommensurate satellite. It would seem that in the misaligned domain the field-induced transition is of first order and that the II-O-IV region corresponds to a mixed-phase state. Indeed, at $T = 1.4$ K we have observed some field hysteresis: on sweeping the external field down from $H = 4$ T the Néel component vanishes and the satellite appears at slightly lower fields, than in the case when the H is gradually increased from zero. We believe that in a perfectly aligned sample the transition must be of second order, in which case the II-O-IV region is replaced by a single line.

E. Measurements of $\zeta(H)$

Accurate measurements of the field dependence of ζ were performed in experiment II where one domain was tilted by $\approx 1°$ (domain A) and the other almost perfectly aligned (domain B). Measurements for domain A could easily be done at base temperature (1.4 K) in a field-cooled sample (Fig. 4, solid circles). Additional data for domain A were collected at $T = 2.4$ K. At this temperature $\zeta(H)$ was found to follow the same curve as at $T = 1.4$ K to within experimental error.

For domain B, experiments in the interesting field region, where ζ starts to decrease rapidly with increasing H, could not be performed at low temperature: the domain itself is destroyed in fields higher than ≈ 1.7 T (see above). Nevertheless, $\zeta(H)$ for domain B could be measured in a zero-field-cooled sample at $T = 2.4$ K, i.e., just at the temperature of the critical point O in the phase diagram. At this temperature the B domain survives up to the critical field and the Néel component does not appear before the $(1+\zeta,-\zeta,0)$ peak vanishes. Apparently even at 2.4 K domain-wall pinning is sufficiently strong and kinetics sufficiently slow to make the energetically less favorable (better aligned) domain metastable even in high fields. This does not happen at low temperature: the commensurate structure emerges in a first-order transition and presumably the thermodynamic force that destroys the better aligned domain is larger. Some typical scans for domain B at $T = 2.4$ K are shown in Fig. 6. The dashed line shows experimental Q resolution. The $(1+\zeta, -\zeta,0)$ satellite is resolution-limited at $H < 1.95$ T [Fig. 6(a)] and starts to gradually broaden at higher fields [Fig. 6(b,c)]. The experimental $\zeta(H)$ is plotted in open circles in Fig. 4. We clearly see the sensitivity of the system to even a minor tilt of the applied field relative to the c axis. While at low fields $\zeta(H)$ for domains A and B coincide, there is a substantial discrepancy near the transition point.

F. Critical indexes

In our previous work we have reported measurements of the order-parameter critical exponent $\beta = 0.145(0.005)$ for
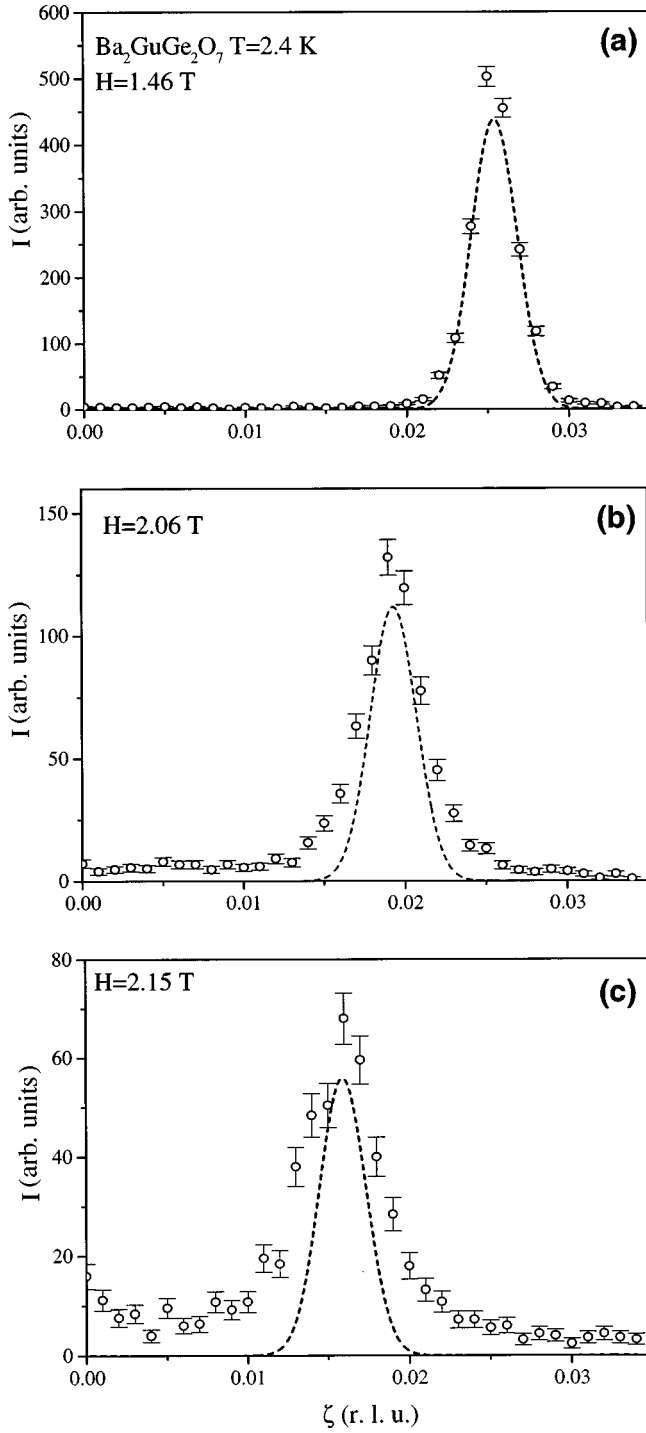
FIG. 6. Elastic scans measured along the $(1+\zeta,-\zeta,0)$ direction in $Ba_2CuGe_2O_7$ at $T=2.4$ K for several values of magnetic field applied along the c axis of the crystal. For this domain the $(1,0,0)$ component does not appear before the critical field is reached.

the zero-field transition from paramagnetic (PM) to spiral states. Having discovered the commensurate phase, we have in addition determined β for the PM $\rightarrow$ commensurate transition at $H=3.66$ T. The intensity of the $(1,0,0)$ magnetic reflection is plotted against $(T_N-T)/T_N$ in a log-log plot in Fig. 7 (open circles). Fitting the data with a power-law dependence we obtain $\beta_{H=4\,T}=0.185(0.005)$. The previously measured temperature dependence of the $(1.0273,0.0273,0)$ Bragg intensity at $H=0$ is shown in solid symbols in Fig. 7.
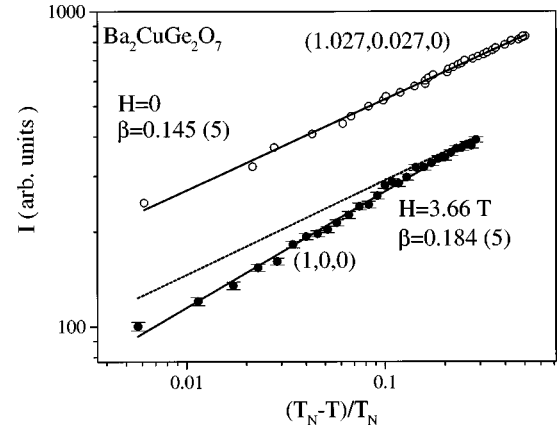

FIG. 7. Measured Bragg intensity of the $(1,0,0)$ (open circles, $H=3.66$ T, $T_N=3.5$ K) and $(1+\zeta,\zeta,0)$ (solid circles, $H=0$, $T_N=3.2$ K) magnetic Bragg reflections. The solid lines are power-law fits to the data. The dashed line is an aid to the discussion in the text.

Although the experimentally determined critical indexes are rather close to each other, in our data we clearly see that $\beta=0.145$ is incompatible with the 4 T measurement (Fig. 7, dashed line).

IV. THEORY

In the introduction section we have qualitatively shown how DM interactions stabilize the magnetic spiral in $Ba_2CuGe_2O_7$ and why applying a field along the c axis of the crystal should result in a commensurate structure. We shall now develop a quantitative description of a DM spin spiral in an external magnetic field. The general expression for the free energy of such a system was obtained by Dzyaloshinskii,[16] who also predicted the CI transition and obtained analytical expressions for the critical properties [at $(H_c-H)/H\ll1$]. In the present work we extend Dzyaloshinskii's approach and derive analytical expressions for the period and the uniform magnetization of the spiral valid throughout the phase diagram. We start by considering a simple, yet illustrative, case of a classical spin chain at $T=0$.

A. Classical spin chain with DM interactions

Let us consider the 1D case: a uniform chain of classical spins with isotropic (Heisenberg) antiferromagnetic exchange. In addition, we include a Dzyaloshinskii energy term with the $\mathbf{D}$ vector pointing along the arbitrary chosen y axis. The system is then characterized by the following Hamiltonian (energy functional):

$$\mathcal{H}=2J\sum_n \mathbf{S}_n\mathbf{S}_{n+1}+\mathbf{D}\sum_n (\mathbf{S}_n\times\mathbf{S}_{n+1})_y. \qquad (1)$$

It is straightforward to show that to take full advantage of the Dzyaloshinskii term, the spins have to be confined to the (x,z) plane. The total interaction energy of a pair of spins is given by $\mathcal{E}=2JS^2\cos\phi+DS^2\sin\phi=S^2\sqrt{4J^2+D^2}\cos(\phi-\alpha)$, where ϕ is the angle between the spins, and α

$=\arctan D/2J\ll1$, provided $J\gg D$. The classical ground state is therefore an AF spiral, where the angle between subsequent spins is equal to $\pi+\alpha$.

Physically interesting behavior occurs when an external magnetic field is applied perpendicular to the Dzyaloshinskii vector **D**, e.g., along the z axis. In this case one has to take into account the Zeeman energy $-Hg\mu_B\Sigma_n S_z$, where g is the gyromagnetic ratio and μ_B is the Bohr magneton. Denoting by ϕ_n the angle the nth spin $\mathbf{S}_n$ forms with the z axis, we can rewrite the energy functional as

$$\mathcal{H}=\sum_n \ [\ \widetilde{J}\cos(\phi_{n+1}-\phi_n-\alpha)-\widetilde{H}\cos\phi_n], \quad (2)$$

where $\widetilde{J}=S^2\sqrt{4J^2+D^2}$ and $\widetilde{H}=Hg\mu_B S$.

In Eq. (2) we clearly see the competing terms that drive the CI transition. The J term favors an incommensurate (spiral) structure, where the phases ϕ_n of subsequent spins differ by $\pi+\alpha$. The effect of the magnetic field is more subtle. For $\widetilde{H}\gg\widetilde{J}$ the spins tend to align parallel to the field. For $\widetilde{H}\ll\widetilde{J}$ however, the system still can gain some Zeeman energy without sacrificing much of its exchange energy. This is achieved in a spin-flop state, where all spins are roughly perpendicular to the magnetic field and are slightly tilted in its direction. The external field thus favors a commensurate spin-flop structure, but it can only be realized by sacrificing some Dzyaloshinskii energy. Indeed, the energy difference between the spin-flop configuration and the spiral state is $\widetilde{J}(1-\cos\alpha)-\widetilde{H}^2/8\widetilde{J}$. The spin-flop state becomes energetically favorable in fields $\widetilde{H}>\widetilde{H}_c\sim2\alpha\widetilde{J}$. This is the simplified physical picture already discussed in the introduction section. The above crude argument does not take into account the *distortion* of the spiral by the applied field. The exact result for our model, $\widetilde{H}_c=\pi\widetilde{J}\alpha$ is derived below.

B. Exact ground state in the continuous limit

It is convenient to change angle variables so that

$$\phi_n=\pi n+\theta_n. \quad (3)$$

The energy functional in this notation becomes

$$\mathcal{H}=\sum_n \ [-\widetilde{J}\cos(\theta_{n+1}-\theta_n-\alpha)-(-1)^n\widetilde{H}\cos\theta_n]. \quad (4)$$

The advantage of the new set of variables is that assuming $\alpha=2\pi\zeta\ll1$ and $\widetilde{H}\ll\widetilde{J}$, the phase difference $\theta_{n+1}-\theta_n-\alpha\ll1$, so we can safely replace the first term in Eq. (4) with $-\widetilde{J}+\widetilde{J}(\theta_{n+1}-\theta_n-\alpha)^2/2$.

The ground state satisfies the extremal conditions $\partial\mathcal{H}/\partial\theta_n=0$, which gives us the following set of equations:

$$\theta_{n+1}+\theta_{n-1}-2\theta_n=\frac{\widetilde{H}}{\widetilde{J}}(-1)^n\sin\theta_n. \quad (5)$$

These equations can be solved in the continuous limit. We shall look for a solution in the form $\theta_n=\Theta(n)+(-1)^n\vartheta(n)$, where both $\Theta(n)$ and $\vartheta(n)$ are functions that only slowly change on the scale of a single lattice spacing.

From Eq. (5) we obtain the extremal condition that should be satisfied in an energy minimum:

$$\frac{d^2\Theta}{dn^2}=-\frac{\widetilde{H}^2}{8\widetilde{J}^2}\sin2\Theta, \quad (6)$$

$$\vartheta=-\frac{\widetilde{H}}{4\widetilde{J}}\sin\Theta. \quad (7)$$

The first of these equations is the famous sine-Gordon equation, which allows for exact soliton solutions. The trivial "no-soliton" solution to Eqs. (6,7) is $\Theta(n)=\pi/2$, and $\vartheta(n)=-\widetilde{H}/4\widetilde{J}$. This is precisely the spin-flop phase, realized in a strong enough magnetic field. Less trivial is the one-soliton solution:

$$\Theta(n)=2\arctan[\exp(n\widetilde{H}/2\widetilde{J})]-\pi/2,$$

$$\vartheta(n)=-\widetilde{H}/4\widetilde{J}\tanh(n\widetilde{H}/2\widetilde{J}), \quad (8)$$

which has boundary conditions $\Theta(-\infty)=-\pi/2$ and $\Theta(+\infty)=\pi/2$.

For $\alpha=0$ the energy of the one-soliton state will be always higher than that of the soliton vacuum (spin-flop state). In the general case, substituting Eq. (8) into the energy functional (4), we find the energy difference between the one-soliton and soliton-free state: $\mathcal{E}_1-\mathcal{E}_0=\widetilde{H}-\widetilde{J}\pi\alpha$. We see that for $\widetilde{H}<\widetilde{H}_c$, where

$$\widetilde{H}_c=\pi\alpha\widetilde{J}=2\pi^2\zeta\widetilde{J},$$

$$H_c=4\pi^2\zeta\frac{JS}{g\mu_B}, \quad (9)$$

the energy of a single soliton is negative and solitons spontaneously "condense." This process will eventually saturate, due to the mutual repulsion of solitons, and the ground state will be a periodic "soliton lattice."

At the non-negligible soliton density the interaction starts to change the shape of individual solitons and has to be taken into account explicitly. Fortunately the general solution of the sine-Gordon equation is known:

$$\int_0^{\Theta(n)}\frac{\beta dx}{\sqrt{1-\beta^2\sin^2 x}}=\frac{n\widetilde{H}}{2\widetilde{J}}, \quad (10)$$

$$\Theta(n)=\mathrm{am}\left(n\frac{\widetilde{H}}{2\widetilde{J}\beta},\beta\right), \quad (11)$$

$$\vartheta(n)=-\frac{\widetilde{H}}{4\widetilde{J}}\sin\Theta(n)=-\frac{\widetilde{H}}{4\widetilde{J}}\mathrm{sn}\left(n\frac{\widetilde{H}}{2\widetilde{J}\beta},\beta\right), \quad (12)$$

where $\mathrm{am}(x,\beta)$ and $\mathrm{sn}(x,\beta)$ are Jacobi elliptic functions of modulus β. Substituting this solution into the energy functional (4) we obtain the interaction energy per spin:

$$\mathcal{E}=\frac{(g\mu_B H)^2}{16J}\left[-\frac{1}{\beta^2}+\frac{2E(\beta)}{\beta^2 K(\beta)}-\frac{2H_c}{\beta HK(\beta)}\right], \quad (13)$$
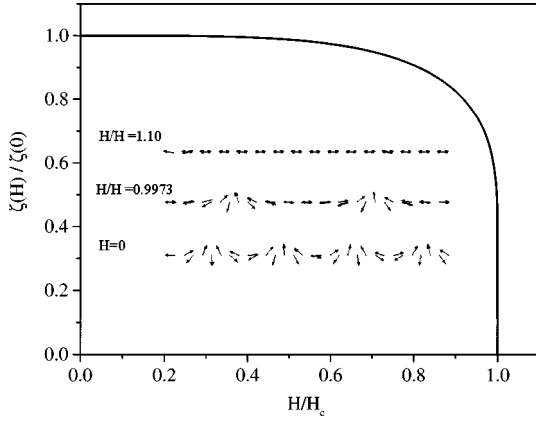
FIG. 8. Theoretical field dependence of the magnetic propagation vector ζ, obtained from an exact solution of a classical one-dimensional antiferromagnet with Dzyaloshinskii-Moriya interactions in the continuous limit. Inset: schematic representation of the spiral phase ($H=0$), soliton lattice ($0<H<H_c$) and the spin-flop commensurate state ($H>H_c$).

where K and E are the complete elliptic integrals of the first and second kind, respectively.

Equation (13), as well as the expression for H_c [Eq. (9)] were derived in Ref. 16. In the present work we go one step further and determine which of the solutions given by Eqs. (11,12) indeed correspond to the ground state at any particular $H<H_c$. Unlike that in Ref. 16, our treatment is not limited to the narrow critical region $(H_c-H)/H_c \ll 1$. Taking the partial derivative of the energy functional (13) with respect to β, and substituting identities for derivatives of elliptic integrals,[18] after some algebra we get

$$\frac{H}{H_c} = \frac{\beta}{E(\beta)}, \qquad (14)$$

$$\mathcal{E} = -\frac{(g\mu_B H)^2}{16J} \frac{1}{\beta^2}. \qquad (15)$$

Equation (14) is to be solved with respect to β for any given H/H_c. $\zeta(H)$ can then be expressed in terms of β:

$$\frac{\zeta(H)}{\zeta(0)} = \frac{H}{H_c} \frac{\pi^2}{4\beta K(\beta)} = \frac{\pi^2}{4E(\beta)K(\beta)}. \qquad (16)$$

Equations (14) and (16) provide us with $\zeta(H)$ in a parametric form. The ratio $\zeta(H)/\zeta(0)$ is plotted against H/H_c in Fig. 8. The inset schematically shows the spin structure for $H=0$, $0<H<H_c$, and $H>H_c$.

At low density soliton repulsion is exponentially small and the system close to the transition point is extremely sensitive to any perturbations of the original Hamiltonian, which will tend to pin down the soliton lattice in one of the metastable configurations. As $H \to H_c-0$, the soliton density decreases as $1/|\ln(H_c-H)|$, i.e., very rapidly.[16] The transition is thus almost first order [the critical exponent $\delta=0$ in $\zeta(H) \sim (H_c-H)^\delta$].

The soliton lattice at $H \neq 0$, unlike the pure sinusoidal spiral at $H=0$, has higher Fourier harmonics at $\zeta_{2n+1} = \pm(2n+1)\zeta(H)$. The knowledge of the exact ground state enables us to calculate these harmonics analytically. For the
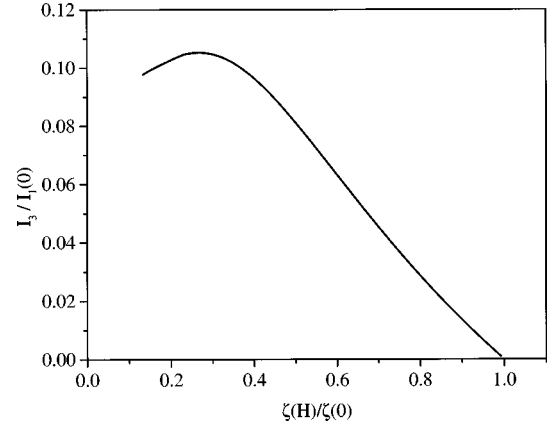

FIG. 9. Theoretically predicted Bragg intensity of the third Fourier harmonic of the soliton lattice plotted as a function of $\zeta(H)/\zeta(0)$.

Bragg intensity (square of the amplitude) of the strongest third harmonic, for example, one gets

$$\frac{I_3(H)}{I_1(H)} = \frac{q^2(1-q^2+q^4)}{(1+q^2+q^4)^2}, \qquad (17)$$

$$\frac{I_3(H)}{I_1(0)} = \frac{2\pi^2[q^3/(1-q^3)^2+q^3/(1+q^3)^2]}{\beta^2 K(\beta)^2}, \qquad (18)$$

where

$$q = \exp\left(-\pi \frac{K(\sqrt{1-\beta^2})}{K(\beta)}\right).$$

This ratio of intensities is plotted against $\zeta(H)/\zeta(0)$ in Fig. 9. Except very close to H_c, all harmonics are much weaker than the first one.

As we derived a parametric expression for $\zeta(H)$, so we can also obtain an exact parametric form for the uniform magnetization $M = -\partial\mathcal{E}/\partial H$. From Eqs. (14,15), and the identities for derivatives of elliptic integrals[18] one gets

$$M = \frac{(g\mu_B)^2 H}{8J} \frac{1}{\beta^2}\left(1 - \frac{E(\beta)}{K(\beta)}\right). \qquad (19)$$

The magnetization curve is continuous at the critical field. On the other hand, its derivative with respect to H (the field-dependent susceptibility) diverges when H_c is approached from below.

C. Generalization to finite temperatures and higher dimensions

The results obtained in the previous chapter can be easily generalized to the cases of higher system dimensionality and finite temperatures. We follow the approach developed by Dzyaloshinskii in Ref. 16 and introduce the expression for the free energy of a general almost antiferromagnetic spiral in an external magnetic field. We generalize the results derived for the 1D chain in the previous section to obtain analytical expressions for the period and the magnetization of the structure valid not only in the critical region, but throughout the phase diagram.

Since the period of the spiral is long, nearest-neighbor magnetic moments are almost opposite to each other. This enables us to approximately describe the structure in terms of position-dependent staggered magnetization $\mathbf{L}(\mathbf{r})$. To take full advantage of the DM interaction, $\mathbf{L}(\mathbf{r})$ must be perpendicular to the DM vector, and therefore be confined to the x-z plane. We further assume that the magnitude $|\mathbf{L}(\mathbf{r})|$ does not depend on $\mathbf{r}$. This simplification is justified since the Zeeman energy, which at H_c is of order of DM interaction energy, is much smaller than the energy of isotropic exchange. The local magnetic structure is thus fully defined by the angle $\theta(\mathbf{r})$, that $\mathbf{L}(\mathbf{r})$ forms with the z axis. The total ''elastic'' free energy per single Cu plane, associated with spin-spin interactions, can then be written as

$$F_{\text{elast}} = \frac{1}{2} \rho_s(T) \int dx\,dy \left[\left(\frac{\partial \theta(\mathbf{r})}{\partial x} - \frac{\alpha}{\Lambda} \right)^2 + \left(\frac{\partial \theta(\mathbf{r})}{\partial y} \right)^2 \right. $$
$$\left. + \gamma \left(\frac{\partial \theta(\mathbf{r})}{\partial z} \right)^2 \right]. \qquad (20)$$

Equation (20) is given in the form suitable for describing a single Cu plane in $Ba_2CuGe_2O_7$. $\rho_s(T)$ is the so-called spin stiffness at given temperature, $\Lambda = \Lambda_{ab}$ is the in-plane nearest-neighbor Cu-Cu distance, and γ is the spin stiffness anisotropy factor, defined as $\gamma(\Lambda_c/\Lambda_{ab})^2 = |J_c|/|J_{ab}| \approx 1/37$ in $Ba_2CuGe_2O_7$. Coordinates x, y, and z run along $(1,1,0)$, $(1,\bar{1},0)$, and $(0,0,1)$ directions, respectively. The spin stiffness at zero temperature is given by $\rho_s(0) = 2JS^2$.[19] As T approaches T_N the spin stiffness decreases as $|\mathbf{L}(\mathbf{r})|^2$ and vanishes precisely at T_N.

In taking into account the external magnetic field, it is convenient to introduce the quantities $\chi_\|(T)$ and $\chi_\perp(T)$, the magnetic susceptibilities of the system with respect to a field that rotates along with the spiral structure and is always parallel or perpendicular to the local staggered magnetization, respectively. As in a usual antiferromagnet, these susceptibilities do not diverge at T_N. In the paramagnetic phase (at $T > T_N$), $\chi_\|(T) = \chi_\perp(T)$. At zero temperature the classical result is $\chi_\perp(0) = (g\mu_B)^2/(8dJ\Lambda^2)$,[19] and $\chi_\|(0) = 0$.

The full expression for the free-energy density in the presence of magnetic field H applied along the z direction is

$$F = F_{\text{elastic}} - \frac{\chi_\perp H^2 \sin^2 \theta(\mathbf{r}) + \chi_\| H^2 \cos^2 \theta(\mathbf{r})}{2}$$
$$= \frac{\rho_s}{2} \left[\left(\frac{\partial \theta(\mathbf{r})}{\partial x} - \frac{\alpha}{\Lambda} \right)^2 + \left(\frac{\partial \theta(\mathbf{r})}{\partial y} \right)^2 + \gamma \left(\frac{\partial \theta(\mathbf{r})}{\partial z} \right)^2 \right]$$
$$- \frac{(\chi_\perp - \chi_\|) H^2}{2} \sin^2 \theta(\mathbf{r}) - \frac{\chi_\| H^2}{2}. \qquad (21)$$

At $T = 0$ and $d = 1$ Eq. (21) coincides with the expression for the energy of a spin chain derived in the previous section.

The equilibrium configuration of $\theta(\mathbf{r})$ minimizes the free energy and therefore satisfies a generalized form of Eq. (6):

$$\frac{\partial^2 \theta}{\partial x^2} = -\frac{(\chi_\perp - \chi_\|) H^2}{\rho_s} \sin\theta \cos\theta = -\frac{1}{2\Gamma^2} \sin 2\theta, \qquad (22)$$

where $\Gamma = [\rho_s/H^2(\chi_\perp - \chi_\|)]^{1/2}$. The critical field is now given by

$$H_c = \pi^2 \zeta(0) \sqrt{\frac{\rho_s}{(\chi_\perp - \chi_\|)\Lambda^2}}. \qquad (23)$$

For a fourth-nearest-neighbor AF like $Ba_2CuGe_2O_7$ at $T = 0$ we can use $\chi_\perp = (g\mu_B)^2/16J\Lambda^2$, $\chi_\| = 0$, and $\rho_s = J_{ab}S^2$. Substituting these expressions into Eq. (23) we obtain

$$H_c = 4\sqrt{2}\zeta\pi^2 \frac{JS}{g\mu_B}, \qquad (24)$$

a factor of $\sqrt{2}$, compared to the 1D case [Eq. (9)]. This factor is due to the fact that in two dimensions each spin is antiferromagnetically coupled to four, rather than two nearest neighbors, and the overall structure is stiffer. Unlike antiferromagnetic in-plane interactions, *ferromagnetic* coupling between adjacent Cu planes in $Ba_2CuGe_2O_7$ does not change $\chi_\perp$ or the expression for the critical field.

The temperature dependence of H_c can be easily understood within the mean-field (MF) approximation. In this framework $\chi_\perp$ is T independent, $\chi_\|$ decreases with $T_N - T$ and $\chi_\perp = \chi_\|$ at $T = T_N$. The effective strength of exchange coupling, represented by JS^2 in Eq. (23) goes as the square of the order parameter, i.e., as $T_N - T$ (the MF order-parameter critical exponent $\beta = 0.5$). Substituting these values in Eq. (23), we find that within the MF approximation H_c is independent of temperature. This result is the same as for the spin-flop field in a conventional easy-axis Heisenberg antiferromagnet.

Finally, we can generalize the expression (19) for the magnetization. With new parameters in the sine-Gordon equation we get

$$M = \chi_\| H + (\chi_\perp - \chi_\|) \frac{H}{\beta^2} \left(1 - \frac{E(\beta)}{K(\beta)} \right), \qquad (25)$$

for $H \leq H_c$. For $H > H_c$ one has $M = \chi_\perp H$. The field-dependent susceptibility $\chi(H) = dM/dH$ is given by

$$\chi(H) = \chi_\| + \frac{(\chi_\perp - \chi_\|)}{\beta^2} \left(1 + \frac{E(\beta)^3}{(1-\beta^2)K(\beta)^3} - \frac{2E(\beta)}{K(\beta)} \right). \qquad (26)$$

At $H = 0$ this expression gives $\chi(0) = (\chi_\perp + \chi_\|)/2$: the structure is a uniform spiral, which effectively averages out the susceptibility for all directions in the spin plane. The susceptibility diverges at H_c as $1/(H_c - H)\ln^2(H_c - H)$.[16] Above H_c it has a constant value equal to $\chi_\perp$.

V. DISCUSSION

A. DM interactions in $Ba_2CuGe_2O_7$

We have shown that the spiral spin arrangement in $Ba_2CuGe_2O_7$ is due to the in-plane component D_y of the Dzyaloshinskii vector $\mathbf{D}$ for nearest-neighbor Cu^{2+} ions. It is rather difficult to experimentally determine whether or not the out-of-plane component D_z is also active. In the spin-flop phase the predicted canted weak-ferromagnetic structure differs from a Néel state only in that it gives rise to additional magnetic peaks coincident with nuclear Bragg reflections. The latter are much stronger than any magnetic scattering intensities, and make measurements of the ferromagnetic component all but impossible. In the spiral phase however, if

$D_z \neq 0$, satellites of type $(h+\zeta, k+\zeta, l)$ should be observable around *ferromagnetic* zone centers, in addition to the principal magnetic peaks positioned around the AF zone centers. In preliminary experiments at $T=1.5$ K we have indeed observed extremely weak elastic features at reciprocal-space positions $(2+\zeta, \zeta, 0)$ and $(1+\zeta, 1+\zeta, 0)$. So far we have not investigated the possibility of these features being artifacts due to nuclear-magnetic double scattering.[20] We plan to resolve this uncertainty in future experiments.

B. The commensurate-incommensurate transition

Studies of CI phase transitions have a long history, dating back to pioneering works of Frenkel and Kontorova[21] and Frank and van der Merwe.[22] Since then CI transitions were discovered and studied experimentally in a number of such seemingly unrelated systems as noble-gas monolayers adsorbed on graphite surface,[23] charge-density-wave materials,[24] ferroelectrics,[25] and rare-earth magnets.[26] (For comprehensive reviews see, for example, Ref. 27.) As a rule, CI transitions result from a competition between two distinct terms in the Hamiltonian that have different ''built-in'' spatial periodicities and are often referred to as potential and elastic energy, respectively. The potential energy by definition favors a structure commensurate with the crystal lattice. Such is the interaction between gas atoms and the graphite matrix in intercalated and adsorbed systems. The elastic term is intrinsic to the system where the transition occurs, and has a different ''natural'' built-in period. For adatoms on graphite this term represents their mutual interaction. In our case of a Heisenberg AF with DM interactions it is the $\widetilde{H}\cos\phi_n$ term in Eq. (2) that plays the role of an effective potential, forcing the spins in the plane, thus favoring a commensurate structure. The competing elastic term is $\widetilde{J}\cos(\phi_{n+1}-\phi_n-\alpha)$, and the ''natural'' periodicity is set by the angle α.

In many known realizations of CI transitions, such as adsorbed gas monolayers, it is the period set by the elastic term that can be varied in an experiment to drive the transition, whereas both the strength and the period of the potential remain constant. In other systems, among them rare-earth magnets, both the elastic term (exchange coupling between spins) and the potential (magnetic anisotropy) can be changed, but only indirectly, by varying the temperature. In both cases one typically observes a ''devil's staircase'' phase diagram (for a review see, for example, Ref. 27): the incommensurate structure tends to lock onto rational fractions of the period of the potential. Instead of continuous CI transitions one gets a series of commensurate-commensurate transitions between different lock-in states.

The interest of Dzyaloshinskii's model for CI transitions is that it is driven by a changing strength of the potential alone, with both built-in periods remaining constant. The experimentalist has a convenient handle on the potential term that he can vary by simply adjusting the external field. Since the ''built-in'' periods do not change, the transition is continuous with no ''devil's staircase'' behavior.

The other advantage of the present realization of CI transitions lies in the fact that the potential energy has a pure sinusoidal form as a function of the angle $\theta(x)$. The model can be exactly solved and a quantitative comparison of theory and experiment are possible for the entire phase diagram. In most other CI systems one knows only that the potential energy is a periodic function with a given period, determined by the underlying lattice, while its exact functional form remains undetermined. Quantitative comparison of experiment and theory in this case is restricted to the narrow critical region close to the transition point.

It is important to note here that while field-induced CI transitions have been previously observed in a number of magnetic insulators with incommensurate structure,[28–30,6] for various reasons none of them is well described by Dzyaloshinskii's model. In FeGe (Ref. 6) the problem is that in the high-symmetry cubic structure applying even a very small magnetic field rearranges the spins so that the spin-rotation plane is perpendicular to the field direction, in violation of Dzyaloshinskii's requirement. Instead of a second-order Dzyaloshinskii transition one gets a first-order spin-flip transition from the incommensurate phase directly into the paramagnetic state. Although this does not happen in compounds like $RbMnBr_3$ (Refs. 28,29) and $CsFeCl_3$,[30] the phase behavior there is seriously complicated by the quantum effects and frustration in the triangular spin lattice.[31]

In the following paragraphs we shall demonstrate that the experimental data on the CI transition in $Ba_2CuGe_2O_7$ agrees with our solution to Dzyaloshinskii's model at the quantitative level. $Ba_2CuGe_2O_7$ thus appears to be the first system that exhibits a Dzyaloshinskii-type transition in its original form.

C. Estimates for the critical field

The appeal of the theory presented above is that it allows for an exact solution. Its major limitation of course is that it is based on a classical, rather than quantum-spin model. Nevertheless, our theoretical predictions seem to be in excellent agreement with what is experimentally observed in $Ba_2CuGe_2O_7$, even at the quantitative level. To begin with, the model gives the correct value for the critical field H_c. The in-plane exchange parameter $J=0.48$ meV was previously determined by measuring the spin-wave dispersion spectrum.[15] The exchange energy per bond is then $\widetilde{J}=2JS^2 \approx 0.24$ meV. The g values were measured in ESR experiments: $g_a=2.044$ and $g_c=2.474$.[32] By substituting $\zeta(0)=0.027$ into Eq. (24) we immediately obtain $H_c=3.3$ T, that should be compared to the experimental value $H_c \approx 2.1$ T. Considering that for the theoretical estimate we used predictions for $T=0$ and ignored quantum effects, a 30% consistency is quite acceptable.

D. The soliton lattice

The most intriguing prediction of our theory for CI transition in $Ba_2CuGe_2O_7$ is that the spin structure close to the phase transition is no longer an ideal spiral, but rather should be viewed as a lattice of solitons, i.e., domain walls separating regions of Néel-like spin arrangement. The soliton lattice is a distinguishing characteristic of all CI systems. Several comprehensive reviews on the subject exist, among them papers by Bak[27] and Pokrovsky *et al.*[33] The basic physical mechanism is quite simple. When the potential term is sufficiently large, but still smaller than the critical value, it is favorable for the system to have large ''commensurate'' re-

gions. The elastic energy from the "incommensurate" term in the Hamiltonian is partially released by forming domain walls or phase slips that separate "commensurate" domains.

From the experimental point of view the soliton lattice concept has three important consequences. The first is that the incommensurability parameter ζ is field dependent, and $\zeta \rightarrow 0$ *continuously* as $H \rightarrow H_c$ (Fig. 8). Moreover, the transition itself is very unusual: continuous, yet logarithmically steep at H_c. The experimental $\zeta(H)$ data collected for the well-aligned domain (Fig. 4, open circles) can be nicely fit by the theoretical curve shown in Fig. 8, treating $\zeta(0)$ and H_c as adjustable parameters. A very good agreement is obtained with $\zeta(0) = 0.027(1)$ and $H_c = 2.13(2)$ T at $T = 2.4$ K (solid line in Fig. 4). All the way up to $\zeta(H)/\zeta(0) \approx 2/3$ the theoretical curve follows the experimental points closely. In the very proximity of H_c however, a deviation is apparent. This is to be expected: the soliton lattice becomes infinitely soft at the transition point and pinning to structural defects leads to a saturation of $\zeta(H)$ at $H \rightarrow H_c$ and effective broadening of magnetic Bragg reflections (Fig. 6). The almost-first-order transition is very fragile. A small misalignment of the field produces what we see in the misaligned domain as a first-order transition with a mixed-phase region and a substantially different form of $\zeta(H)$ in the vicinity of H_c.

Inherently related to the unusual logarithmic phase transition is an anomaly in the magnetic susceptibility at H_c. We have used the theoretical expression (25) to fit the experimental $\chi(H)$ shown in Fig. 2. Since we cannot explicitly take into account the quantum and thermal spin fluctuations, we have treated $\chi_\parallel$, $\chi_\perp$, and H_c as independent fitting parameters. In addition, we allowed for a linear term vH in $\chi(H)$ that is present in both the $\mathbf{H} \| \mathbf{a}$ and $\mathbf{H} \| \mathbf{c}$ data. This term empirically accounts for intrinsic nonlinearities in magnetization curves in the quantum (quasi) two-dimensional AF Heisenberg model (Ref. 34, especially Fig. 5), that in our case effectively modify the local susceptibilities $\chi_\perp$ and $\chi_\parallel$ at high fields. The fit is shown in a solid line in Fig. 2. The values of the fitting parameters are: $\chi_\parallel = 0.89 \times 10^{-5}$ emu/g, $\chi_\perp = 3.43 \times 10^{-5}$ emu/g, $v = 1.72 \times 10^{-10}$ emu/g, and $H_c = 1.88$ T. This value for H_c obtained from magnetization at $T = 2$ K is slightly lower than $H_c = 2.13(2)$ T obtained from neutron diffraction at $T = 2.4$ K.

Finally, an important feature of the magnetic structure at finite fields is that it no longer is an ideal sinusoidal spiral. As discussed above, this distortion is characterized by higher-order Bragg harmonics, which should be observable in neutron-diffraction experiments. Although we have spent some time looking for the third-order magnetic satellite during experiment II, at $T = 2.4$ K and for several values of applied field, we were so far unable to find it. The reason is probably the lack of intensity. As can be seen from Fig. 9, the relative intensity of the third harmonic is very small except in the immediate proximity of H_c, where the first satellite itself is broadened and weakened. We would like to emphasize here that the form of $\zeta(H)$ and the existence of higher-order harmonics are *in essence one and the same effect*. Since theory agrees so well with experiment as far as $\zeta(H)$ is concerned, we are confident in that satellites are present and will be observed in future experimental efforts.

E. System dimensionality

We finally comment on our measurements of critical exponents. In our previous work we have shown that there are several hints, including the temperature dependence of magnetic susceptibility, to that $Ba_2CuGe_2O_7$ should primarily be considered a two-dimensional antiferromagnet. This is further confirmed by the measured order-parameter critical exponent $\beta = 0.184$ for the PM$\rightarrow$ commensurate transition, i.e., substantially smaller than in standard 3D models, where $\beta > 0.3$ for Heisenberg, XY and even Ising systems. One could naively expect that at high external fields the critical index would be *smaller* than at $H = 0$, since the symmetry of the corresponding Hamiltonian is smaller. Exactly the opposite is observed experimentally. The only suggestion that we can make at this point is that $Ba_2CuGe_2O_7$ falls into a completely different universality class than conventional magnets. Considering the nature of the spiral phase and DM interactions, we may be dealing with one of the chiral universality classes.[35] To obtain further insight into the critical properties of $Ba_2CuGe_2O_7$ further field-dependent measurements of the of β and other critical indexes are required.

No matter what the observed critical exponents are, the long-range magnetic ordering is still a purely three-dimensional phenomenon. For a CI occurring at finite temperature dimensionality is known to play a key role. In a purely 1D system at nonzero temperature the ground state will be destroyed, since the energy required to create a soliton is finite while the entropy gain proportional to $\ln L$ is infinite in the thermodynamic limit. Solitons will be spontaneously created at any temperature and no sharp transition will occur. In two dimensions, the effect of thermal (or quantum) fluctuations is more subtle. For a general case Pokrovskii, Talapov, and Bak have demonstrated that the effective soliton-soliton interaction is altered by fluctuations.[33] The short-range exponential repulsion $\exp(-\lambda r)$ is replaced by a long-range term $1/r^2$. This modifies the behavior close to the transition point, making the phase transition the usual second-order-type with $\zeta(H) \sim (H_c - H)^{1/2}$. Only in three dimensions should the results that we have derived for the ground state remain valid at finite temperatures. The transition in this case is of almost first order, with logarithmic "corrections" near the transition point making it continuous.

F. Ideas for future experiments

$Ba_2CuGe_2O_7$ is a very interesting system, yet it is relatively easy to investigate experimentally. The Heisenberg exchange constants are small, so the magnon-dispersion relations could be measured in the entire Brillouin zone. DM interactions are relatively strong and the incommensurability parameter $\zeta(0)$ is sufficiently large to be easily measurable. $H_c \approx 2$ T is also readily accessible in most types of experiment, even those that require the use of diffraction-adapted horizontal-field magnets. The work on $Ba_2CuGe_2O_7$ is far from being completed. The first priority is to find the higher-order harmonics of the incommensurate magnetic peaks and study the temperature dependence of their intensities. One should also look for satellites around ferromagnetic zone centers to see if there is a weak-ferromagnet distortion of the spiral structure. The effect of a magnetic field applied in the (a,b) plane is worth investigating. The critical behavior is

not fully understood and accurate field-dependent measurements of all critical indexes are highly desirable. Finally, it would be interesting to look at dynamical properties of the soliton lattice. Near the critical field the soliton-soliton interaction is extremely weak, which gives rise to spin waves with very low velocity.

VI. CONCLUSION

We have observed a rare type of CI transition in an antiferromagnetic insulator with Dzyaloshinskii-Moriya interactions. The transition is driven exclusively by the changing strength of the commensurate potential. The latter is directly controlled in an experiment by varying the magnetic field. A transition of this kind was envisioned over three decades ago

by Dzyaloshinskii, and we have now found that $Ba_2CuGe_2O_7$ exhibits it in its original form. In addition, we have extended Dzyaloshinskii's theoretical treatment to derive exact parametric equations for the field dependence of magnetization and incommensurability vector.

[1] I. E. Dzyaloshinskii, Sov. Phys. JETP **5**, 1259 (1957).
[2] I. E. Dzyaloshinskii, J. Exp. Theor. Phys. **46**, 1420 (1964).
[3] T. Moriya, Phys. Rev. **120**, 91 (1960).
[4] P. Anderson, Phys. Rev. **115**, 2 (1959).
[5] C. Wilkinson, F. Sinclair, and J. B. Forsyth (unpublished).
[6] B. Lebech, J. Bernhard, and T. Flertoft, J. Phys.: Condens. Matter **1**, 6105 (1989).
[7] Y. Ishikawa, K. Tajima, D. Bloch, and M. Roth, Solid State Commun. **19**, 525 (1976).
[8] Y. Ishikawa, T. Komatsubara, and D. Bloch, Physica B **86–8**, 401 (1977).
[9] Y. Ishikawa and M. Arai, J. Phys. Soc. Jpn. **53**, 2726 (1984).
[10] M. Hase, I. Terasaki, and K. Uchinokura, Phys. Rev. Lett. **70**, 3651 (1993).
[11] M. Hase *et al.*, Phys. Rev. B **48**, 9616 (1993).
[12] Y. Sasago *et al.*, Phys. Rev. B **52**, 3533 (1995).
[13] A. Zheludev *et al.*, Phys. Rev. B **53**, 11 642 (1996).
[14] Y. Sasago, K. Uchinokura, A. Zheludev, and G. Shirane, Phys. Rev. B **55**, 8357 (1997).
[15] A. Zheludev *et al.*, Phys. Rev. B **54**, 15 163 (1996).
[16] I. E. Dzyaloshinskii, Sov. Phys. JETP **20**, 665 (1965).
[17] A. Zheludev, S. Maslov, G. Shirane, Y. Sasago, N. Koide, and K. Uchinokura, Phys. Rev. Lett. **78**, 4857 (1997).
[18] I. S. Gradstein and I. M. Ryzhik, *Tables of Integrals, Series, and Products* (Academic, New York, 1980), Eq. (8.123).
[19] S. Chakravarty, B. Halperin, and D. Nelson, Phys. Rev. B **39**, 2344 (1989).
[20] R. M. Moon and C. G. Shull, Acta Crystallogr. **17**, 805 (1964).
[21] Y. Frenkel and T. Kontorova, Zh. Eksp. Teor. Fiz. **8**, 1340 (1938).
[22] F. Frank and J. van der Merwe, Proc. R. Soc. London, Ser. A **198**, 205 (1949).
[23] R. Clarke, in *Ordering in two dimensions*, edited by S. Sinha (North-Holland, Amsterdam, 1980), p. 53; H. Zabel, *ibid.*, p. 61.
[24] J. A. Wilson, F. J. DiSalvo, and S. Mahajan, Adv. Phys. **24**, 117 (1975).
[25] A. H. Moudden, E. C. Svensson, and G. Shirane, Phys. Rev. Lett. **49**, 557 (1982).
[26] W. C. Koehler, in *Magnetic Properties of Rare Earth Metals*, edited by R. J. Eliott (Plenum, New York, 1972), p. 81.
[27] P. Bak, Rep. Prog. Phys. **45**, 587 (1982).
[28] L. Heller, M. F. Collins, Y. S. Yang, and B. Collier, Phys. Rev. B **49**, 1104 (1994).
[29] M. Zhitomirsky, O. Petrenko, and L. Prozorova, Phys. Rev. B **52**, 3511 (1995).
[30] W. Knop, M. Steiner, and P. Day, J. Magn. Magn. Mater. **31-34**, 1033 (1983).
[31] T. Nikuni and A. E. Jacobs, cond-mat/9702201, Phys. Rev. B (to be published 1 March 1998).
[32] Y. Sasago (unpublished).
[33] V. L. Pokrovsky, A. L. Talapov, and P. Bak, in *Solitons*, edited by S. E. Trullinger, V. E. Zakharov, and V. L. Pokrovsky (Elsevier Science, Amsterdam, 1986), Chap. 3.
[34] K. Fabricius, M. Karbach, U. Löw, and K.-H. Mútter, Phys. Rev. B **45**, 5315 (1992).
[35] H. Kawamura, Phys. Rev. B **38**, 4916 (1988).